
This is an electronic reprint of the original article.
This reprint may differ from the original in pagination and typographic detail.

Välisalmi, Teemu; Bettahar, Houari; Zhou, Quan; Linder, Markus B.
Pulling and analyzing silk fibers from aqueous solution using a robotic device

Published in:
International Journal of Biological Macromolecules

DOI:
[10.1016/j.ijbiomac.2023.126161](https://doi.org/10.1016/j.ijbiomac.2023.126161)

Published: 01/10/2023

Document Version
Publisher's PDF, also known as Version of record

Published under the following license:
CC BY

Please cite the original version:
Välisalmi, T., Bettahar, H., Zhou, Q., & Linder, M. B. (2023). Pulling and analyzing silk fibers from aqueous solution using a robotic device. *International Journal of Biological Macromolecules*, 250, Article 126161. <https://doi.org/10.1016/j.ijbiomac.2023.126161>

This material is protected by copyright and other intellectual property rights, and duplication or sale of all or part of any of the repository collections is not permitted, except that material may be duplicated by you for your research use or educational purposes in electronic or print form. You must obtain permission for any other use. Electronic or print copies may not be offered, whether for sale or otherwise to anyone who is not an authorised user.



Pulling and analyzing silk fibers from aqueous solution using a robotic device

Teemu Välisalmi^{a,c}, Houari Bettahar^b, Quan Zhou^{b,*}, Markus B. Linder^{a,c,**}

^a Department of Bioproducts and Biosystems, School of Chemical Engineering, Aalto University, FI-00076 Aalto, Finland

^b Department of Electrical Engineering and Automation, School of Electrical Engineering, Aalto University, FI-00076 Aalto, Finland

^c Centre of Excellence in Life-Inspired Hybrid Materials (LIBER), Aalto University, P.O. Box 16100, FI-00076 Aalto, Finland

ARTICLE INFO

Keywords:
Spidroin
Protein fiber
Liquid-liquid phase separation

ABSTRACT

Spiders, silkworms, and many other animals can spin silk with exceptional properties. However, artificially spun fibers often fall short of their natural counterparts partly due sub-optimal production methods. A variety of methods, such as wet-, dry-, and biomimetic spinning have been used. The methods are based on extrusion, whereas natural spinning also involves pulling. Another shortcoming is that there is a lack feedback control during extension. Here we demonstrate a robotic fiber pulling device that enables controlled pulling of silk fibers and in situ measurement of extensional forces during the pulling and tensile testing of the pulled fibers. The pulling device was used to study two types of silk—one recombinant spider silk (a structural variant of ADF3) and one regenerated silk fibroin. Also, dextran—a branched polysaccharide—was used as a reference material for the procedure due to its straightforward preparation and storage. No post-treatments were applied. The pulled regenerated silk fibroin fibers achieved high tensile strength in comparison to similar extrusion-based methods. The mechanical properties of the recombinant spider silk fibers seemed to be affected by the liquid-liquid phase separation of the silk proteins.

1. Introduction

Spiders, silkworms, and many other animals spin silk for various purposes with the ultimate goal to increase their likelihood of survival [1,2]. Thus, the spun silk fibers have exceptional properties tailored for specific purposes [2–5]: e.g., lacewing silk is rigid, especially in lateral dimension, to allow the egg stalks made from silk to stand out of the reach of predators and be resistant to bending [4], while flagelliform silk from spiders lacks strength it is extremely ductile to aid in entangling and snaring preys [3,5]. The silk fiber that has been gathering the most interest is the supporting component of the spider web called spider dragline silk, which is known for its toughness—the combination of high strength and ductility [3,5]—that exceed most industrial fibers [3,5,6]. In addition, the natural silk spinning process takes place at ambient temperature and pressure [2,5], it requires no solvents [2,3,5,6], and is highly energy efficient [6]. This combined with its exceptional mechanical properties makes spider silk a promising candidate for a sustainable biomaterial for industrial production. However, natural properties of the spider silk fibers have been difficult to replicate in vitro

[3,6,7], due to various reasons, such as the complicated structure of the silk proteins and lack of understanding of the material formation process [3,7].

The main component of dragline spider silk, major ampullate silk proteins (MaSp) are generally very large, hundreds of kDa, and contain repetitive units of polyalanine and glycine-rich stretches [3,5,7,8]. The mechanical properties of the silk fiber are linked to these repetitive units: long polyalanines correlate with high tensile strength while long glycine-rich stretches increase flexibility [3]. Due to the limitations of common expression systems like *Escherichia coli*, the repetitive full-length silk proteins are expressed poorly [7]. Thus, often shorter MaSp are chosen for recombinant silk protein production, such as ADF3 from *Araneus diadematus* (~60 kDa) [9], or engineered recombinant silk that contain a number of repeats from MaSp, such as AQ12 (12 repeats from ADF3) [10], 4RepCT (4 repeats from MaSp1 of *Euprosthrops australis*) [11], or N-R12-C (12 repeats from MaSp2 of *Trichonephila clavipes*) [12]. Recombinant production opens possibilities for further engineering of the silk protein. For example, the terminal domains of the silk protein can be replaced with other globular proteins to provide additional

* Corresponding author.

** Correspondence to: M.B. Linder, Department of Bioproducts and Biosystems, School of Chemical Engineering, Aalto University, FI-00076 Aalto, Finland.

E-mail addresses: quan.zhou@aalto.fi (Q. Zhou), markus.linder@aalto.fi (M.B. Linder).

<https://doi.org/10.1016/j.ijbiomac.2023.126161>

Received 24 April 2023; Received in revised form 3 August 2023; Accepted 4 August 2023

Available online 6 August 2023

0141-8130/© 2023 The Authors. Published by Elsevier B.V. This is an open access article under the CC BY license (<http://creativecommons.org/licenses/by/4.0/>).

functions, such as enhanced affinity to cellulose [13] or other biomolecules [14]. Also, some recombinant silks have been observed to self-assemble into liquid-like droplets called coacervates via liquid-liquid phase separation (LLPS), which has been proposed to be an important step in the formation of molecular structures that lead to different biological functions [12,13,15–17].

While silkworm *Bombyx mori* silk is not as astounding in its mechanical properties as dragline silk [5,6], its availability makes it a valuable resource for experimental work. *B. mori* fibers consist of proteins fibroin light chain (~25 kDa), fibroin heavy chain (350 kDa), fibroin p25, and different sericin proteins [8,18]. Like spidroins, fibroin heavy chain contains repetitive units [8]. These consist of repeats of glycine and alanine segments (GA) that are separated by nonrepetitive regions [8]. Large quantities of reconstituted fibroin can be acquired from *B. mori* cocoons for example by boiling the cocoons in sodium carbonate to remove sericin, dissolving the silk in a chaotropic agent, and finally removing the chaotropic agent via dialysis resulting in re-generated silk fibroin (RSF) solution [19].

There are four general strategies for artificial spinning of silk fibers: wet spinning, dry spinning, electrospinning, and biomimetic spinning [3,5,6]. In wet spinning a silk/solvent mixture is extruded into a coagulant bath, such as ethanol, isopropanol, or ammonium sulphate, which solidifies the fiber via coagulation [3,6]. Wet spinning of RSF [20–23] and recombinant silk [7,9,24–26] are well studied in literature, but this method comes with the downside of requiring the use of coagulants and has the potential drawback of resulting in sub-optimal properties due to forced precipitation of the silk protein [3,27]. Electrospinning also involves coagulant baths or organic solvents but results in nonwoven mats instead of individual fibers [3,6]. In dry spinning the liquid-solid transition happens in air due to the evaporation of the organic or aqueous solvent [28,29]. While less popular than wet spinning, dry spinning of RSF is moderately documented [28–34]. For example, Sun et al. spun aqueous RSF, and post treated the fibers with ethanol coagulant and drawing at different ratios: non treated (as-spun) fibers had a breaking strength of 45.7 ± 2.5 MPa and breaking strain of 2.1 ± 0.6 % while post treated fibers varied between 123.5 and 150.8 MPa and 21–31.1 % depending on the drawing parameters [30]. Studies of recombinant silk dry spinning on the other hand are lacking, and only few similar studies can be found where the fiber is pulled in air from a small droplet [13,35]. A new development is biomimetic spinning, which is influenced by the natural spinning mechanism [3,5]. In the silk gland the silk dope is moved through a thinning spinning duct while being subjected to chemical (e.g., pH, ion content, dehydration) and physical (shear) changes [3,5]. While otherwise similar to wet spinning, biomimetic spinning differs in that no harsh solvents are used. Several studies have been reported on biomimetic spinning: [27,36,37]. For example, Schmuck et al. extruded recombinant silk (NT2RepCT in aqueous buffer, pH 8) into an acidic aqueous buffer solution (pH 5), resulting in fibers with a breaking strength up to 100 MPa and elongation of 100 % [36].

While all of these studies provide valuable information on how the different silk-based materials can be spun, it has been pointed out that *B. mori* silk is likely dominantly pulled instead of pushed due to the lack of internal forces, such as osmotic pressure or peristalsis capable of creating enough pressure for spinning of silk dope just by extrusion [38]. Similar in-depth studies have not been conducted with spiders, but it has been pointed that pulling also plays a major part in the spinning of the spider silk [3,39,40]. The pulling process is difficult to reproduce artificially since the force and rate of pulling is controlled by internal feedback regulation and will affect final properties. Instruments used for artificial pulling generally lack such feedback control.

Thus, in this study we used a robotic fiber pulling device for controlled pulling and tensile testing of silk fibers. We used two different silks—RSF and an AQ12-based recombinant silk—and dextran as a reference material. The robotic pulling device measured the force during fiber pulling and the strength of the final fibers. The force measurements were used to study correlations between the mechanical properties of

the fibers and other parameters, such as force during the hardening of the fiber and pulling velocities. No post treatments were applied.

2. Materials and methods

2.1. Recombinant silk expression and purification

The recombinant spider silk protein (referred to as “recombinant silk”) used in this study is a silk-like protein with a triblock structure CBM-AQ12-CBM (85 kDa). The mid-block is an engineered silk protein sequence called AQ12 [10], which contains 12 repetitive repeats from the major ampullate gland silk fibroin 3 (ADF3) of *A. diadematus*. The mid-block is flanked at both N and C-terminus by a cellulose binding module (CBM) from *Ruminiclostridium thermocellum*. Although here CBM functionality was not used, adding the CBMs help to increase production yields and makes the protein easier to process [13]. A polyhistidine tag (6× His) is attached to the end of the C-terminus for affinity purification. The cloning procedure has been described previously [13].

The recombinant silk was expressed in *Escherichia coli* (BL21 strain). EnPresso B500 media was used for protein expression according to the manufacturer's protocol (EnPresso GmbH). The cells were harvested after 24 h of induction (10,000 rcf, 10 min), and lysed by sonication (50 % amplitude, 5 min with 2 s pulses). The lysate was heated (30 min, 70 °C), which led to the precipitation and easy removal of most non-target proteins, and then further purified by nickel affinity chromatography ÄKTA-Pure using HisTrap FF crude columns (GE Healthcare Life Science). The eluted recombinant silk was desalted using Econo-Pac 10DG columns (Bio-Rad) and distilled water. The desalted recombinant silk was concentrated to 5–15 wt% using 30 kDa cut-off polyethersulfone membrane centrifugal concentrators (Vivaspin, Sartorius). The protein concentration was determined by UV absorption at 280 nm (NanoDrop, Thermo Fisher Scientific) using an extinction coefficient of 1.266. The concentrated recombinant silk solutions were stored at room temperature for at most 24 h before use.

2.2. Regeneration of native silk fibroin

RSF solution was prepared from cocoons of *B. mori* provided by the Agricultural and Environmental Research Center of Italy (CREA-AA). The regeneration protocol was based on the protocol by Rockwood et al., [19] with some modifications. The cocoons were cut into small pieces (~2 × 2 mm), blended in distilled water, and degummed with 0.02 M Na₂CO₃ (70 °C, 30 min) while blending every 5 min. The silk was rinsed with distilled water 3 times for 20 min and dried overnight. The dry silk was mixed with 9.6 M LiBr (4 mL per gram of silk) and incubated at 70 °C for 10 min while mixing continuously. The mixture was transferred to a dialysis tube with 10 kDa molecular weight cut-off (SnakeSkin, Thermo Scientific) and it was dialyzed against distilled water with a constant flow of 0.5 L/h for at least 2 days at 8 °C. The dialysis was continued until conductivity reached 5 µS/cm (Jenway 4520). The RSF was concentrated to 10–15 wt% using 10 kDa cut-off polyethersulfone membrane centrifugal concentrators (Vivaspin, Sartorius). The concentration of RSF was determined by drying aliquots at 80 °C and weighing them. Concentrated RSF samples were stored at 4 °C for at most 2 days. For additional information (images and videos) of the procedure of the RSF preparation we have made available separately documented data showing the procedure in detail [41].

2.3. Preparation of dextran

Dextran with molecular weight of 500 kDa (Alfa Aesar) was used to prepare 40–70 wt% dextran solutions. Dextran was weighted in a 2 mL Eppendorf tube and distilled water was added to reach the target dextran concentration. The mixture was uniformly dispersed using a spatula. The mixture was incubated at room temperature overnight. The solution was then centrifuged (15,000 rcf, 10 min) to remove air

bubbles. The dextran solutions were quickly frozen using liquid nitrogen and stored at $-20\text{ }^{\circ}\text{C}$.

2.4. Setup of the robotic fiber pulling device

The experimental setup shown in Fig. 1a was designed to implement autonomous pulling of fibers from different materials, and to perform tensile testing without removal of the fiber. The setup is an improved version of a previously described one [42,43]. It consisted of a syringe held on a motorized precision positioner (Physik Instrumente, model M404.4PD) (number 6 in Fig. 1a). The plunger of the syringe was connected to a second motorized precision positioner (number 8 in Fig. 1a). A blunt glass needle (diameter 1 mm) was attached on the syringe. A force sensor (load range 10 g, accuracy 0.0082 g, LCM Systems, model LCM UF1) was fixed at the top of the device. A pointed tip was attached to the force sensor, facing towards the needle. The two motorized precision positioners were operated via a controller (Physik Instrumente, model C-884.4CD) using Matlab/Simulink. The force sensor was connected to a data acquisition (DAQ) board (National Instrument, model PCIe-6363). The setup was constructed on a vibration isolation table. Two cameras were installed on the side to record the experiment: one camera (FLIR, Model CM3-U3-50S5M-CS) to observe the tip of the glass needle from the side and other camera (FLIR, model GS3-U3-51S5M-C) to record the complete experiment from a sideview.

2.5. Pulling and tensile testing of fibers

The experimental protocol of fiber pulling and tensile testing (Fig. 1b, Supporting Information Video S1) was divided in four steps, as follows: (1) dispensing sample from the syringe so that the glass needle was filled, after which the syringe stage was raised until the pointed tip of the force sensor touched the sample. (2) Pulling the fiber by lowering the syringe stage at a given speed until target fiber length was achieved and allowing the fiber to harden. (3) Releasing any load on the fiber formed during the hardening by raising the syringe stage until the measured force reached zero. (4) Tensile testing by lowering the syringe stage at a constant speed until the fiber broke. Force measurements and video images were recorded throughout the experiment. Fig. 1c shows an example of the measured force and displacement of the syringe stage during a typical experiment. Data for the stress-strain curve (Fig. 1d) were obtained from the tensile test step initially as force (N) and then converted into stress (Pa) by dividing by the cross-sectional area of the fiber as described in Materials and Methods 2.6. The experiments were performed at $40 \pm 6\%$ relative humidity and $20 \pm 1\text{ }^{\circ}\text{C}$.

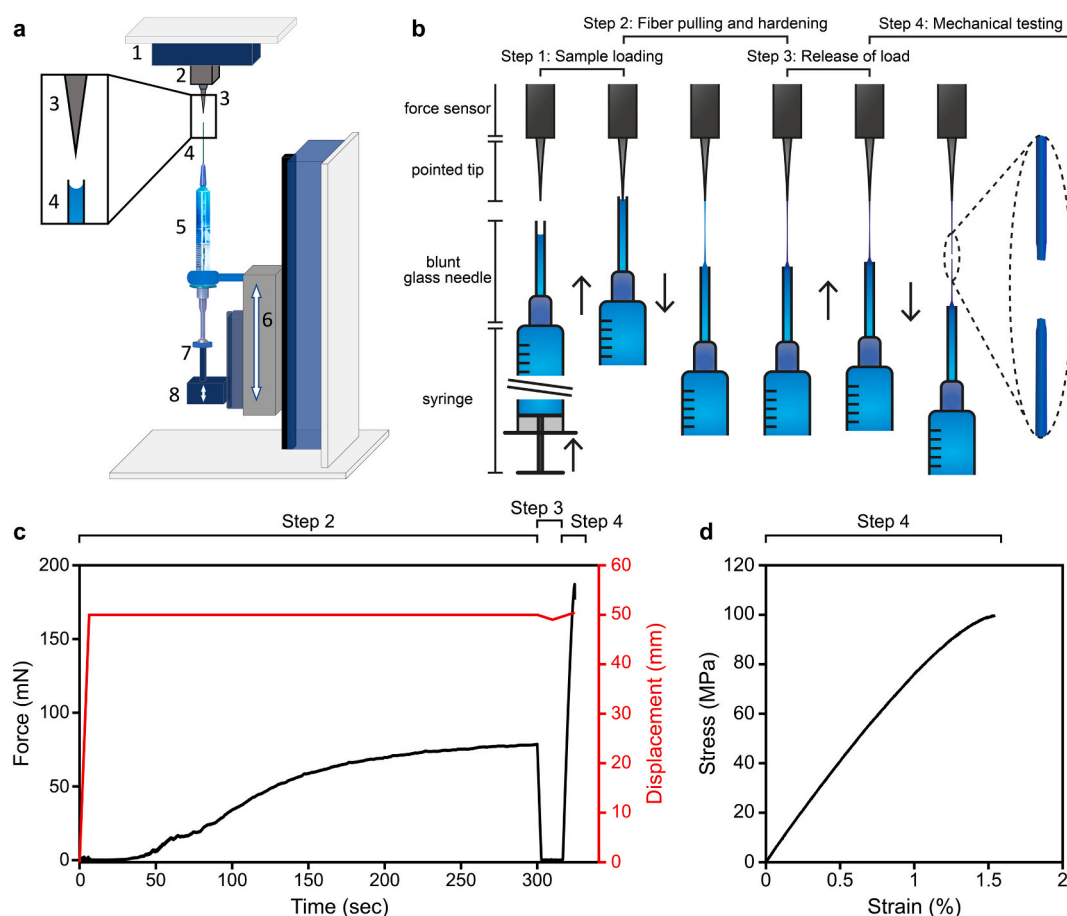


Fig. 1. (a) The experimental setup of the robotic fiber pulling device, which consists of: (1) a manual positioner for adjusting force sensor, (2) a force sensor, (3) a pointed tip connected to force sensor, (4) a glass needle, (5) a syringe, (6) the first precision positioner, (7) a plunger, (8) a second precision positioner to move the plunger. The syringe stage consists of parts 4–8. (b) Fiber pulling and tensile testing consists of four steps: (step 1) dispensing sample from the syringe to fill the glass needle and lifting the syringe stage until there is contact between the pointed tip of the force sensor and the sample, (step 2) pulling the fiber by lowering the syringe stage until the target fiber length is achieved and allowing the fiber to harden, (step 3) releasing tension on the fiber and then (step 4) performing the tensile test. Illustrations are not drawn to scale. (c) Example of the measured force and the displacement of the syringe stage during the experiment from step 2 to step 4. (d) Example of a stress-strain curve obtained from a tensile test and calculated using the cross-sectional area of the fiber obtained from the scanning electron microscope. This part corresponds to step 4.

2.6. Scanning electron microscopy and measurement of the cross-sectional area of the fibers

The fibers were imaged with Zeiss Sigma VP scanning electron microscope (SEM). To measure the cross-sectional area, the fibers were attached on the side of a 10 mm high aluminum stub (12.5 mm diameter) with carbon tape so that the cross-sectional area was pointing upwards. For other imaging, the fibers were attached sideways on top of an aluminum stub with carbon tape. The samples were sputter-coated with 8 nm of gold/palladium and the SEM images were taken by using an acceleration voltage of 1.5 kV and an SE2 detector.

Fibers from each tensile test were collected and the tips of the fractured fibers were imaged. Then, roughly 0.5–1.0 mm of the fiber tip, including the necked region of the fiber, was removed with sharp scissors as illustrated in Fig. 2, and the remaining non-necked area was imaged. The cross-sectional areas of the fibers were obtained from the SEM images by using the open-source software ImageJ. The non-necked cross-sectional areas were used for computing the stress-strain curves (e. g., engineering strength). By imaging long sections of the fibers, it was confirmed that they had uniform thickness along their lengths.

3. Results

3.1. Preliminary tests with recombinant silk, RSF and dextran

Concentrations from 5 to 15 wt% of recombinant silk and RSF in distilled water were prepared to roughly estimate at what concentration it was possible to pull fibers straight from the silk solution. Pulling was briefly tested by placing a droplet of silk between a pair of tweezers and extending the silk. A concentration above 10 wt% of RSF was found to be sufficient to reliably form silk fibers. Recombinant silk formed fibers also at 10 wt%, but with more difficulty than at higher concentrations. Thus, 15 wt% was chosen for the following experiments. Also, to provide a reference polymer melt, solutions from 40 to 70 wt% of polysaccharide dextran (500 kDa) in distilled water were prepared. Below 50 wt% dextran, fibers were difficult to draw and above 65 wt% dextran had poor solubility and started to show strongly elastic behavior. Therefore, a concentration of 60 wt% dextran was chosen. While solutions of recombinant silk, RSF and dextran were all colorless and translucent to the naked eye, under the light microscope they differed notably (Fig. 3): recombinant silk contained coacervate droplets, RSF contained

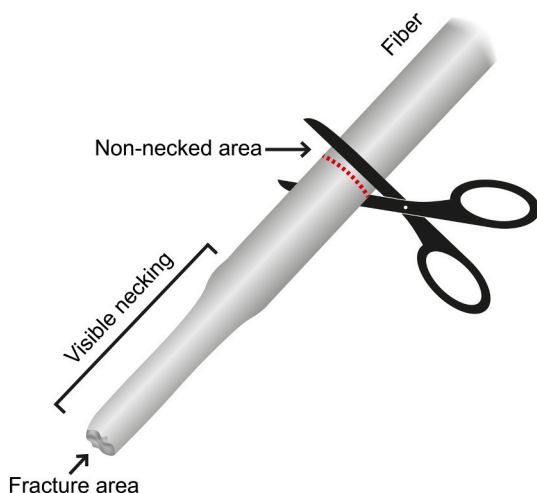


Fig. 2. Illustration of the tip of the fiber after breaking in the tensile test. First, the fracture area was imaged with SEM and then the necked region caused by local plastic deformation was cut off using scissors and the non-necked area was imaged. The cross-sectional area of the non-necked region was used for calculating the mechanical properties. The illustration is not drawn to scale.

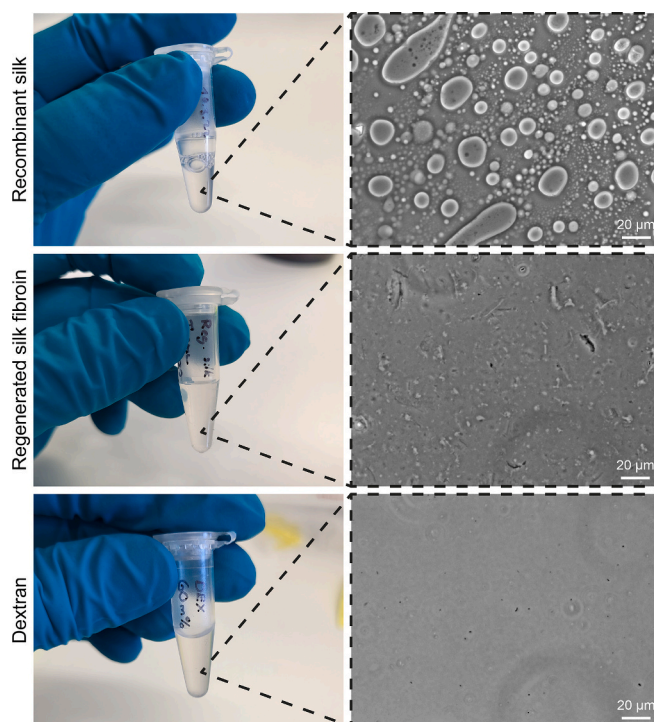


Fig. 3. Microscopy images of the recombinant silk, regenerated silk fibroin (RSF) and dextran solutions. All solutions were fully transparent to the naked eye. Under the microscope recombinant silk (~15 wt%) contained coacervate droplets. The RSF solution (~15 wt%) contained small solid aggregates. The dextran solution (60 wt%) was clear and contained only few visible particles.

numerous small and irregularly shaped particles, and dextran was clear with few visible particles that were likely contaminants. SDS-PAGE of the recombinant silk and RSF are shown in Supporting Fig. S1.

3.2. Recombinant silk, RSF, and dextran fibers

Each material was loaded into a syringe and placed in the fiber pulling device. First, the pulling speeds were selected for the recombinant silk, RSF, and dextran. Each material had a range of pulling speeds at which fibers could successfully be drawn. This range for recombinant silk was 0.2–0.75 mm/s, for RSF it was 0.11–0.25 mm/s, and for dextran it was 15 mm/s up to the maximum speed of the device, which was 50 mm/s (Supporting Information Fig. S2). Some of the fibers were collected for determination of the mechanical properties, but no difference was noticed between the pulling speed and the mechanical properties of the RSF (p -value 0.332) and dextran (p -value 0.981) fibers (Supporting Information Fig. S3). Pulling speeds of 0.5, 0.15, and 25 mm/s were chosen for recombinant silk, RSF, and dextran, respectively.

Next, three batches of each material were applied to the pulling device and pulled into fibers using the parameters obtained from the initial tests, and characterized by tensile testing. However, due to the variation in the properties of the recombinant silk between batches, only one batch resulted in successful fiber pulling. This variation is discussed further below. The fibers were imaged with SEM. Examples of the cross-sectional areas of typical fractured fibers are shown in Fig. 4. All fibers made with recombinant silk showed notable local plastic deformation (i. e., necking) near the fracture point. Generally, the distance between the fracture and necking point was within tens of μm , but in some cases it was up to hundreds of μm (Supporting Information Fig. S4). In contrast, most of the RSF fibers showed no necking except for some very thin fibers. The fracture area of the recombinant silk fibers did not have any distinguishable surface patterns, while RSF fibers often had web-like surface patterns. Dextran fibers were generally hollow and showed

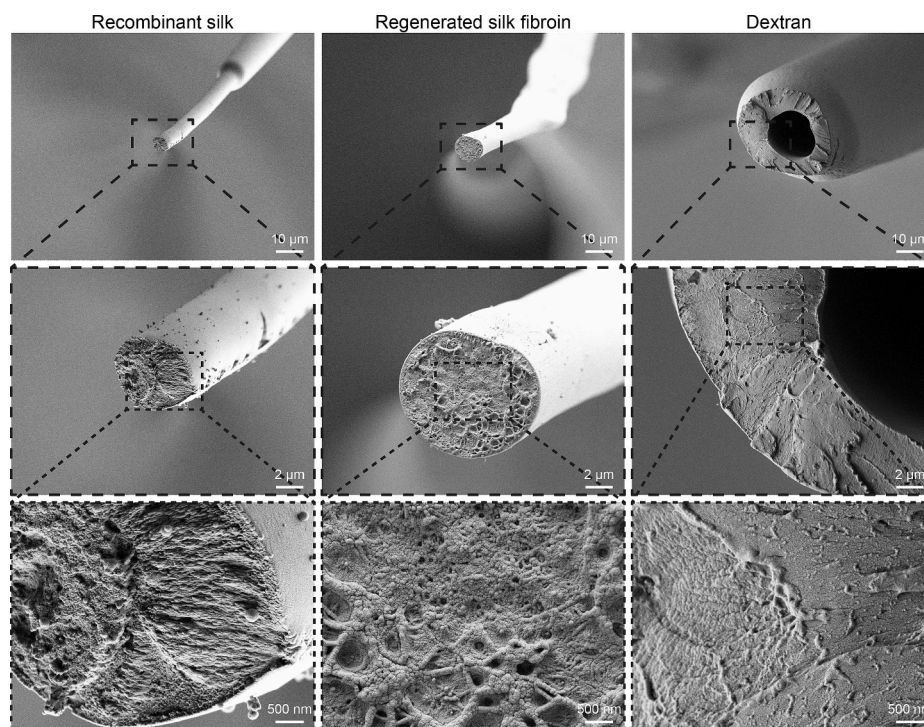


Fig. 4. SEM images of typical fracture surfaces of recombinant silk, regenerated silk fibroin (RSF), and dextran fibers. The recombinant silk fibers showed strong local plastic deformation (necking) near the fracture point. Most of the RSF fibers showed no necking at all. The recombinant silk fibers did not show any specific surface structure at the fracture point, while RSF fibers often had web-like patterns. The dextran fibers were hollow and showed slight necking at the fracture point.

slight necking at the fracture point. The necked regions of the fibers were removed, and the fibers were imaged by SEM again. Representative images of cross-sectional areas of the fractured and non-necked regions are shown in Fig. 5. The area and diameter values of the non-necked fibers are shown in Table 1. The recombinant silk fibers were extremely thin and were barely visible to the naked eye. The cross-sectional areas of the non-necked RSF fibers were approximately an order of magnitude larger than the recombinant silk fibers, while the areas of the dextran fibers were an order of magnitude larger than the RSF fibers.

SEM images of the sides of the fibers are shown in Fig. 6. Fibers were generally smooth, but they had some distinguishable surface features. The recombinant silk fibers had small round particles deposited on them (approx. $126 \text{ nm} \pm \text{SD } 43 \text{ nm}$ diameter), while RSF fibers showed grooves running parallel to the fiber direction. Dextran fibers were generally flattened, likely due to collapse of the hollow core. The surface of the dextran fibers had a bumpy structure that lacked any orientation.

3.3. Mechanical properties of fibers

Tensile testing was used to study differences between the recombinant silk, RSF and dextran fibers, and to find correlations between different parameters and mechanical properties, such as the effect of pulling speed and ultimate (engineering) strength. The tensile tests were done in the pulling device without removing the fiber. After the fiber had been pulled and hardened, it was allowed briefly to relax, after which the tensile test was started by using a speed of 0.2 mm/s for all samples. The resulting stress-strain curves are shown in Fig. 7, and the results are summarized in Table 2. The recombinant silk fibers showed a short elastic region followed by a plastic deformation with up to 4 % strain, but without visible strain hardening. Measurements with recombinant silk were challenging as the forces were close to the sensitivity limit of the force sensor and problems due to the detachment of the fiber from either side. The RSF fibers showed heterogenous results with the ultimate strength varying from 20.7 to 800.6 MPa (median 146.5

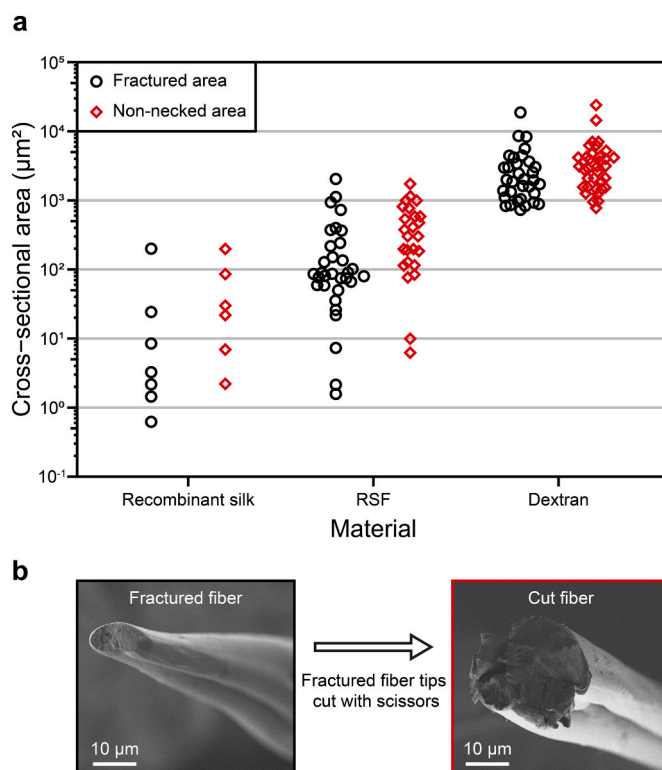


Fig. 5. Fractured and non-necked cross-sectional areas of the recombinant silk, regenerated silk fibroin (RSF), and dextran fibers. (a) Fibers were collected after the tensile test and imaged using SEM before and after removing the necked region of the fiber. Cross-sectional areas were determined using the software ImageJ. Data points were jittered horizontally with increasing width when more data points were near the same value. (b) Example of a fiber before and after removing the necked region.

Table 1

Diameters and cross-sectional areas of the non-necked recombinant silk, regenerated silk fibroin (RSF) and dextran fibers.

Material	Diameter (μm)			Area (μm^2)		
	Median	Average	SD	Median	Average	SD ^a
Recombinant silk	5.7	7.1	5.2	25.8	57.4	75.0
Regenerated silk fibroin	21.0	21.4	11.5	376.0	470.6	437.4
Dextran	60.7	65.1	27.9	3097.5	4040.5	4258.5

^a Sample groups were positively skewed and did not follow the normal distribution. Therefore, SD values can be higher than average values.

MPa) and the strain from 0.4 to 13 % (median 2.6 %). Three RSF fibers differed significantly from the rest, and showed 645.2 MPa ultimate strength with 10.8 % strain, 800.6 MPa ultimate strength with 4.8 % strain, and 122 MPa ultimate strength with 13.0 % strain. Interestingly, these outstanding fibers showed similar necking behavior as the recombinant silk fibers (example in Supporting Information S5). However, it is possible that error in cross-sectional measurement may inflate values of the extremely thin RSF fibers to some degree. All dextran fibers were brittle with an average ultimate strength of $102.4 \text{ MPa} \pm \text{SD } 24.1 \text{ MPa}$ and strain of $1.2 \% \pm \text{SD } 0.2 \%$. The dextran fibers did not show any plastic deformation. The RSF and dextran fibers attached more strongly than the recombinant silk and were held securely during the tensile testing.

3.4. Correlations between the mechanical properties

We next investigated if there was a correlation between the fiber cross-sectional area and the mechanical properties in order to better understand the behavior of the RSF and dextran fibers in the tensile tests. Ultimate strengths as a function of the cross-sectional areas of the RSF and dextran fibers are shown in Fig. 8. We observe that thinner fibers generally gave higher ultimate strength values. For dextran fibers this relationship is more linear. The RSF fibers show mostly a similar relationship, but it is turned into a more exponential correlation by two very thin fibers. It seems that cross-sectional areas between 10 and $200 \mu\text{m}^2$ result in similar ultimate strengths. Correlations between the cross-sectional areas and other mechanical properties of RSF and dextran are shown in Supporting Information Fig. S6–8 (strain, toughness, Young's modulus). The toughness and Young's modulus display similar descending relationship with increasing cross-sectional area, while strain shows more random behavior.

The fiber pulling device allowed measurement of the extensional force also during hardening of the fiber—step 2 in Fig. 1B. During this

hardening step the fiber length was fixed between the pointed tip of the force sensor and the needle. At the start of the hardening step, the extensional force increased rapidly but then slowed down until it reached a plateau, as shown in Fig. 1C. The force was caused by shrinking and hardening of the fiber, which increased tension on the force sensor. The measured force was converted to stress to account for the variation in the cross-sectional area of the fibers. Correlations between the maximum stress during hardening of the fiber and the ultimate strength from the tensile test for the RSF and dextran fibers are shown in Fig. 9. The dextran fibers showed a directly proportional relationship between the ultimate strength and the maximum stress during hardening. The RSF fibers also showed an overall similar relationship, but most of the data points were closely clustered at low values. Interestingly, for both materials the ultimate strength was roughly twice the value of the maximum stress during hardening. In contrast, for the recombinant silk fibers the ultimate strength was six-fold that of the maximum stress during hardening (Supporting Information Fig. S9). Correlations between the maximum stress during hardening and other mechanical properties of the RSF and dextran fibers are shown in Supporting Information Fig. S10–12 (strain, toughness, Young's modulus). The strain and toughness of the RSF fibers displayed no meaningful correlation with the maximum stress during hardening. The strain of dextran fibers increased slightly with the decrease of the maximum stress during hardening, while the toughness showed a slight increase. The Young's modulus of both materials was directly proportional to the maximum stress during hardening.

3.5. Effect of liquid-liquid phase separation on fibers

Three batches of the recombinant silk were expressed and purified. While the batches were produced using the same method and had similar protein concentrations at the end of the purification, they underwent LLPS very differently (Fig. 10), likely due to minor variations in the preparation conditions. The concentrated recombinant silk from batch #1 was full of coacervates that showed coalescence into bigger droplets (up to hundreds of μm in diameter). Batch #2 contained some small coacervates, but most of the visible particles were aggregates with sizes less than $1 \mu\text{m}$ up to hundreds of μm . Batch #3 contained a mixture of small coacervates (up to $20 \mu\text{m}$ in diameter) and some small sub-micron aggregates. In the initial experiments of testing the fiber pulling with tweezers, it was possible to pull fibers from both coacervated and aggregated recombinant silk solutions without noticeable differences. However, when applying the different batches to the pulling device, only fibers from the batch #1 showed forces high enough to be measured and resulted in successful pulling experiments. Some experiments, however, failed when fibers detached during the tensile testing. It was

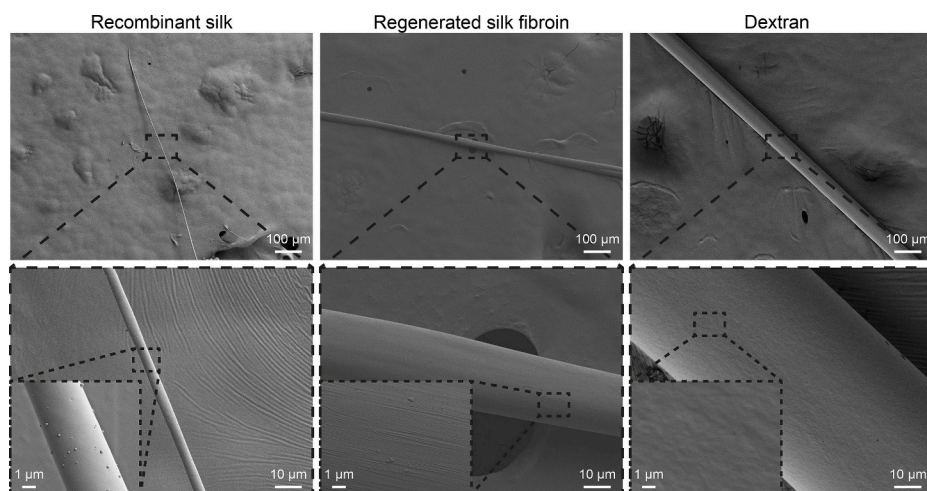


Fig. 6. SEM images of the sides of the recombinant silk, regenerated silk fibroin (RSF), and dextran fibers. Fibers were generally smooth and of the same dimension throughout the fiber but had some distinguishing surface features. The surface of the recombinant silk fibers had depositions of small round particles of approx. $126 \text{ nm} \pm \text{SD } 43 \text{ nm}$ in diameter, and the RSF fibers showed grooves running parallel to the fiber direction. The dextran fibers had a bumpy surface structure that lacked any orientation.

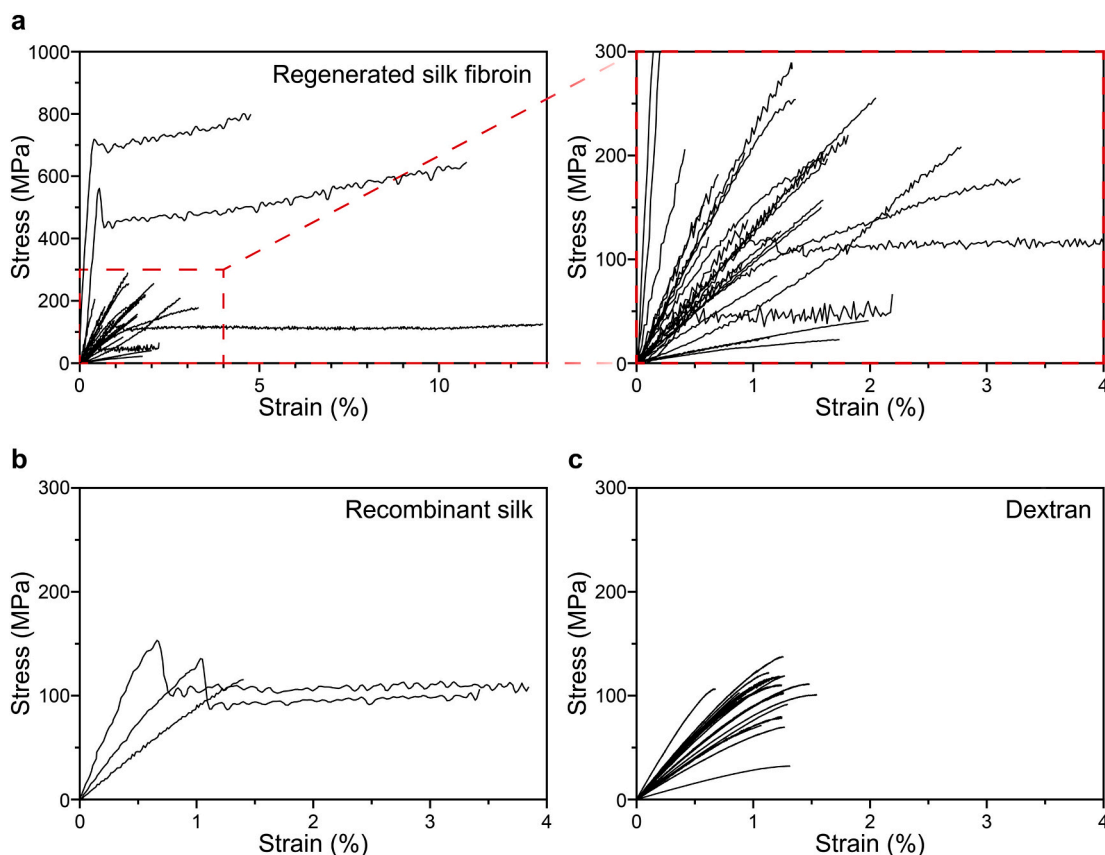


Fig. 7. Stress-strain curves of regenerated silk fibroin (RSF), recombinant silk and dextran fibers. (a) RSF fibers showed ultimate strength from 20.7 to 800.6 MPa and from 0.4 to 13 % strain. (b) Recombinant silk fibers showed high yield stress up to 150 MPa and plastic deformation up to 4 % strain, but without strain hardening. (c) Dextran fibers were brittle with average stress of 102.4 MPa \pm SD 24.1 MPa and strain of 1.2 % \pm 0.2 %.

Table 2
Mechanical properties of recombinant silk, regenerated silk fibroin (RSF) and dextran fibers.

Material	Ultimate strength (MPa)			Strain (%)			Toughness (MJ/m ³)			Young's modulus (GPa)		
	Median	Average	SD	Median	Average	SD	Median	Average	SD	Median	Average	SD
Rec. silk	140.2	141.3	23.4	3.5	2.9	1.3	3.3	2.9	1.8	12.9	14.9	7.7
RSF ^a	146.5	182.9	173.8	2.6	2.9	2.8	1.0	4.7	10.9	10.4	24.4	44.6
RSF ^b	140.6	140.4	78.9	2.2	2.0	0.9	0.9	1.3	1.0	10.3	10.8	6.8
Dextran	104.7	102.4	24.1	1.2	1.2	0.2	0.8	0.7	0.2	9.3	9.2	3.2

^a Sample group positively skewed and did not follow the normal distribution. Therefore, SD values can be higher than average values.

^b Excluding values of the three exceptional fibers.

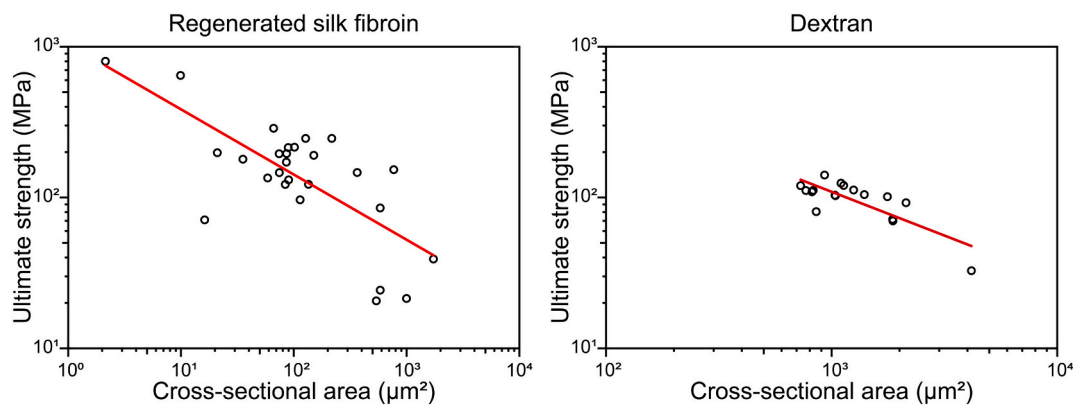


Fig. 8. The effect of the cross-sectional areas of regenerated silk fibroin and dextran fibers to their corresponding ultimate strength values. The results show that thinner fibers generally achieve higher ultimate strength.

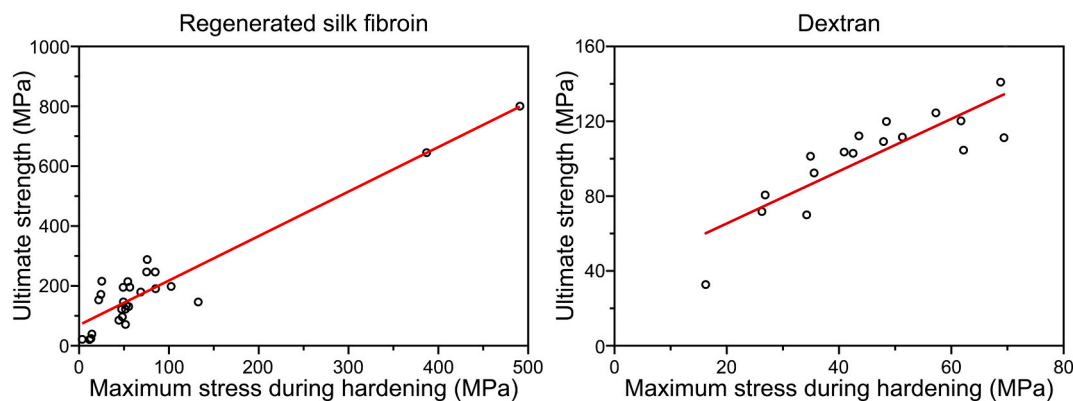


Fig. 9. Correlation between maximal stress during the hardening step in fiber formation and ultimate strength in tensile tests of regenerated silk fibroin and dextran fibers.

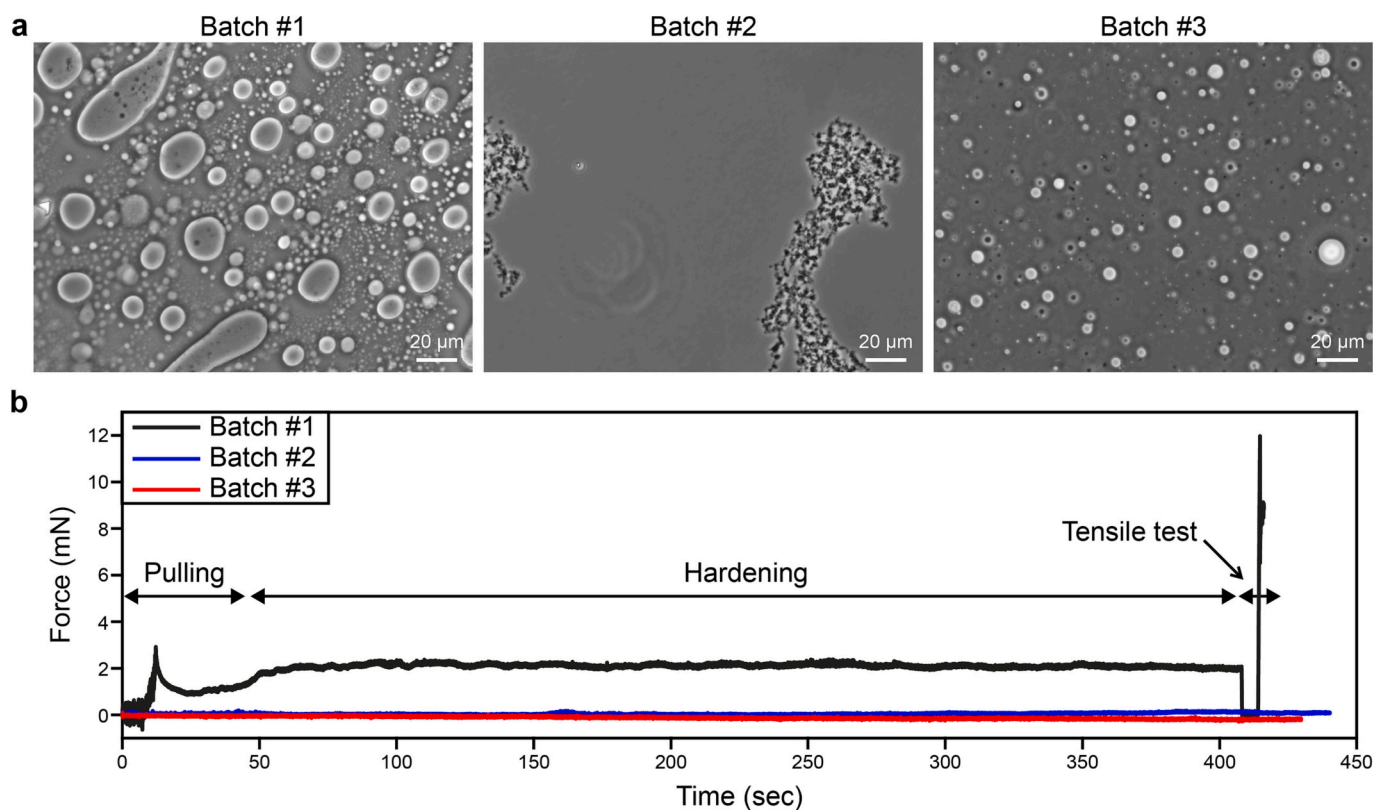


Fig. 10. (a) Microscopy images of the recombinant silk from different expression batches. Batch #1 contained numerous coacervates that showed coalescence into bigger droplets. Batch #2 contained some small coacervates, but most of the particles were aggregates up to hundreds of μm in size. Batch #3 contained mix of small coacervates and aggregates. (b) Examples of the force graph of the fiber pulling experiment. Fibers from batch #1 showed high enough forces to be readily measured. While it was also possible to pull fibers from batches #2 and #3, the forces were below the detection limit of the force sensor.

also possible to pull fibers from the batch #2 and #3. However, the force measurements for the fibers from batch #2 were below the detection limit of the force sensor. For batch #3 occasional small forces were detected but none provided information from the tensile test due to very low forces or detachments.

4. Discussion

The designed robotic fiber pulling device performed well with RSF allowing autonomous processing from loading of the sample up to tensile testing. The pulled RSF fibers showed notable mechanical properties considering that no post-modification was applied (Fig. 7, Table 2). A

comparison to other extrusion-based dry spun RSF fibers without post-modifications—termed as-spun—in the literature, showed that results for the RSF fibers in this study were high. The ones reported here had a median ultimate strength of 146.5 MPa (average 182.9 MPa). For comparison, previously reported average values for as-spun RSF fibers are: 123.5 MPa [29], up to 63 MPa [31], ~ 50 MPa [32], and 78.9 MPa [33]. The notable difference in average and median values in our results was caused by several exceptional fibers that achieved ultimate strengths of up to 800 MPa. These fibers had very small cross-sectional areas (Fig. 5, Fig. 8) and showed much greater plastic deformation and strain hardening in comparison to the rest of the RSF fibers (Fig. 7, Supporting Information Fig. S5). The long deformation shows that the

strongest fibers were qualitatively different than the weaker ones. This can be because the strength of the weak fibers was limited by defects, and never reaching the strains necessary for plastic deformations. The strong outliers would be from solutions that were exceptionally homogenous and without aggregates. Other sources of error can be due to uncertainties in measurement of cross-sectional areas, but such measurement errors would not explain the large plastic deformation. Outliers such as reported here have not been reported in other studies. The heterogeneity of the RSF could be a result of the centrifugal concentration method. Generally, RSF is concentrated by air drying [19,29–33]. Unexpectedly, we noticed that the pulling speed did not seem to affect the mechanical properties of the formed RSF fibers (Supporting Information Fig. S3). Previously, the take up speed of the fiber in extrusion-based spinning methods has been shown to affect the mechanical properties of RSF [23,31].

Our experiments with recombinant silk proteins were faced with multiple complications, such as problems with detachment of the fibers, low forces, and variability in the composition of the recombinant silk samples. The differences in LLPS between the three batches were likely caused by minor differences in the preparation conditions: e.g. cell and silk protein concentration at the end of the cultivation, residues carrying over the affinity purification, degree of aggregation during purification, and starting concentration prior to concentrating. LLPS is known to be susceptible to changes in its environment, such as DNA/RNA [44–46], salts [13,46–48], and protein concentration [13,46,49]. The general variability in LLPS formation is widely observed [15] for this type of protein. The differences occur in sample preparation in which LLPS is triggered by concentration increase, were probably kinetic aspects and nucleation of LLPS lead to different outcomes. The successful experiments showed high average ultimate strength of 141.3 MPa (Fig. 7, Table 2). In comparison, Mohammadi et al. [13] succeeded in pulling fibers by hand from different recombinant silk proteins, including CMB-AQ12-CBM. These showed an average ultimate strength of 16 MPa for fibers with diameters of ranging from 8 to 200 μm . In contrast, in the current study, the fibers were much thinner with an average diameter of 7.1 μm (median 5.7 μm) (Fig. 5, Table 1). The diameters of natural dragline fibers are 2–6 μm [8]. In addition, our results suggests that the LLPS of the recombinant silk affects the mechanical properties of the silk fibers, as samples that showed high amount of coacervates gave the strongest fibers (Fig. 10). This observation is shared with other studies suggesting that LLPS is important for assembly of molecular structures [12,13,15–17]. Thus, better control of the LLPS of the recombinant silk could be a route for solving problems with low forces and variability in the sample composition.

Post-modification can be important for improving the mechanical properties of silk fibers. This is done for example by applying ethanol treatment and post-drawing to enhance crystallinity and molecular alignment [29,31–33]. Also, recent findings suggest that inducing molecular orientation prior to fiber formation could lead to better mechanical performance [6]. Therefore, it is not surprising that the tension during drying had correlation with mechanical properties (Fig. 9). In future work, accurate post-stretching could be applied by controlling this tension. Similarly, chemical post treatment could be implemented by adding solvents in the form of mist or vapor as shown by Koepfel et al. [50].

The recombinant silk fibers showed a strong plastic deformation (Fig. 7). Interestingly, no strain hardening was observed. Strain hardening is known to be a property arising from polymer entanglement [51]. Also, the necking observed in the recombinant silk fibers (Fig. 4, Supporting Information Fig. S4) could suggest lack of strain hardening since necking occurs when the local stresses acting on the fiber cause local strain further accelerating the effect if the rate of strain hardening is insufficient [52]. This interpretation leads to a conclusion that there is a lack of molecular entanglement in the recombinant silk fibers. Polymer size is known to increase entanglement [53], indicating a difference of the relatively short sequence used here as compared to the native one.

On the other hand, Schmuck et al. showed notable strain hardening with biomimetic spun 33 kDa recombinant silk NT2RepCT, which is much shorter [36]. In the NT2RepCT, however a dimerization of both NT and CT domains occur which can lead to long continuous chains that can be more entangled [54].

This work demonstrates the importance of fiber formation mechanisms when studying new materials such as engineered silks. The technical difficulties are numerous, and we found that especially sample preparation is crucial for successful experiments. By working on the technique for fiber formation, in particular fiber pulling, there is a large potential to increase the performance of new molecularly engineered silk-based materials.

Additional videos and images of preparation of the regenerated silk fibroin can be found here: [41].

CRediT authorship contribution statement

H.B. and Q.Z. designed the robotic pulling device and devised a fiber-pulling protocol for studying the effect of hardening stress on tensile properties. H.B. constructed the pulling device. T.V. planned the materials to be tested and did wet-end sample preparation. H.B. did the pulling experiments and collected the data while T.V. loaded the samples into the syringes. After pulling experiments H.B processed the data and T.V collected and characterized fiber samples. All authors participated in data interpretation and analysis. T.V. drafted the main manuscript. H.B. drafted Sections 2.4 and 2.5 and the figures related to the robotic pulling device, force measurements, and mechanical properties. All authors provided feedback on the manuscript and T.V. coordinated finalization. Q.Z. and M.B.L supervised the work.

Funding sources

This work was supported by the Academy of Finland through the following four projects: AI spider silk threading (ASSET) in the AIPSE program (projects #317018 and #317019), project # 317395, and the Center of Excellence Program (2022–2029) in Life-Inspired Hybrid Materials (LIBER) (project #346105). The work was also supported by the Novo Nordisk Foundation (project #0061306).

Declaration of competing interest

The authors declare that they have no known competing financial interests or personal relationships that could have appeared to influence the work reported in this paper.

Acknowledgments

The authors thank Dr. Alessio Saviane (CREA-AA, Italy) for providing *B. mori* cocoons, Dr. Chris Holland for useful advice how to make regenerated silk, and Jennifer Tersteegen for the help with expression of the recombinant silk protein. The authors acknowledge the provision of facilities and technical support by Aalto University at OtaNano - Nanomicroscopy Center (Aalto-NMC) and the Bioeconomy Infrastructure at Aalto University.

Abbreviations

CBM	cellulose binding module
DAQ	data acquisition
LLPS	liquid-liquid phase separation
RSF	regenerated silk fibroin
SEM	scanning electron microscopy

References

- [1] T.D. Sutherland, J.H. Young, S. Weisman, C.Y. Hayashi, D.J. Merritt, Insect silk: one name, many materials, *Annu. Rev. Entomol.* 55 (1) (2010) 171–188, <https://doi.org/10.1146/annurev-ento-112408-085401>.
- [2] F. Vollrath, D.P. Knight, Liquid crystalline spinning of spider silk, *Nature* 410 (6828) (2001) 541–548, <https://doi.org/10.1038/35069000>.
- [3] A. Rising, J. Johansson, Toward spinning artificial spider silk, *Nat. Chem. Biol.* 11 (5) (2015) 309–315, <https://doi.org/10.1038/nchembio.1789>.
- [4] S. Weisman, et al., Fifty years later: the sequence, structure and function of lacing cross-beta silk, *J. Struct. Biol.* 168 (3) (2009) 467–475, <https://doi.org/10.1016/j.jsb.2009.07.002>.
- [5] M. Heim, D. Keerl, T. Scheibel, Spider silk: from soluble protein to extraordinary fiber, *Angew. Chem. Int. Ed.* 48 (20) (2009) 3584–3596, <https://doi.org/10.1002/anie.200803341>.
- [6] A. Koeppel, C. Holland, Progress and trends in artificial silk spinning: a systematic review, *ACS Biomater. Sci. Eng.* 3 (3) (2017) 226–237, <https://doi.org/10.1021/acsbomaterials.6b00669>.
- [7] X.-X. Xia, Z.-G. Qian, C.S. Ki, Y.H. Park, D.L. Kaplan, S.Y. Lee, Native-sized recombinant spider silk protein produced in metabolically engineered *Escherichia coli* results in a strong fiber, *Proc. Natl. Acad. Sci.* 107 (32) (2010) 14059–14063, <https://doi.org/10.1073/pnas.1003366107>.
- [8] M. Andersson, J. Johansson, A. Rising, Silk Spinning in Silkworms and Spiders, *Int. J. Mol. Sci.* 17 (8) (2016) 1290, <https://doi.org/10.3390/ijms17081290>.
- [9] A. Lazaris, et al., Spider silk fibers spun from soluble recombinant silk produced in mammalian cells, *Science* 295 (5554) (2002) 472–476, <https://doi.org/10.1126/science.1065780>.
- [10] D. Huebner, C.W. Helsel, S. Quedzuweit, J. Oschmann, R. Rudolph, T. Scheibel, Primary structure elements of spider dragline silks and their contribution to protein solubility, *Biochemistry* 43 (42) (2004) 13604–13612, <https://doi.org/10.1021/bi048983q>.
- [11] M. Hedhammar, et al., Structural properties of recombinant nonrepetitive and repetitive parts of major Ampullate Spidroin 1 from *Euprostenopsis australis*: implications for fiber formation, *Biochemistry* 47 (11) (2008) 3407–3417, <https://doi.org/10.1021/bi702432y>.
- [12] A.D. Malay, T. Suzuki, T. Katashima, N. Kono, K. Arakawa, K. Numata, Spider silk self-assembly via modular liquid-liquid phase separation and nanofibrillation, *Sci. Adv.* 6, no. 45 (2020), eabb6030, <https://doi.org/10.1126/sciadv.abb6030>.
- [13] P. Mohammadi, et al., Phase transitions as intermediate steps in the formation of molecularly engineered protein fibers, *Commun. Biol.* 1 (1) (2018) 86, <https://doi.org/10.1038/s42003-018-0090-y>.
- [14] R. Jansson, et al., Recombinant spider silk genetically functionalized with affinity domains, *Biomacromolecules* 15 (5) (2014) 1696–1706, <https://doi.org/10.1021/bm500114e>.
- [15] L. Lemetti, J. Tersteegen, J. Sammaljärvi, A.S. Aranko, M.B. Linder, Recombinant spider silk protein and delignified wood form a strong adhesive system, *ACS Sustain. Chem. Eng.* 10 (1) (2022) 552–561, <https://doi.org/10.1021/acssuschemeng.1c07043>.
- [16] J.H. Exler, D. Hümmerich, T. Scheibel, The amphiphilic properties of spider silks are important for spinning, *Angew. Chem. Int. Ed.* 46 (19) (2007) 3559–3562, <https://doi.org/10.1002/anie.200604718>.
- [17] U.K. Slotta, S. Rammensee, S. Gorb, T. Scheibel, An engineered spider silk protein forms microspheres, *Angew. Chem. Int. Ed.* 47 (24) (2008) 4592–4594, <https://doi.org/10.1002/anie.200800683>.
- [18] Y. Takasu, T. Hata, K. Uchino, Q. Zhang, Identification of Ser2 proteins as major sericin components in the non-cocoon silk of *Bombyx mori*, *Insect Biochem. Mol. Biol.* 40 (4) (2010) 339–344, <https://doi.org/10.1016/j.ibmb.2010.02.010>.
- [19] D.N. Rockwood, R.C. Preda, T. Yücel, X. Wang, M.L. Lovett, D.L. Kaplan, Materials fabrication from *Bombyx mori* silk fibroin, *Nat. Protoc.* 6 (10) (2011) 1612–1631, <https://doi.org/10.1038/nprot.2011.379>.
- [20] S. Sohn, S.P. Gido, Wet-spinning of osmotically stressed silk fibroin, *Biomacromolecules* 10 (8) (2009) 2086–2091, <https://doi.org/10.1021/bm900169z>.
- [21] J. Yan, G. Zhou, D.P. Knight, Z. Shao, X. Chen, Wet-spinning of regenerated silk fiber from aqueous silk fibroin solution: discussion of spinning parameters, *Biomacromolecules* 11 (1) (2010) 1–5, <https://doi.org/10.1021/bm900840h>.
- [22] G.R. Plaza, et al., Correlation between processing conditions, microstructure and mechanical behavior in regenerated silkworm silk fibers, *J. Polym. Sci. Part B Polym. Phys.* 50 (7) (2012) 455–465, <https://doi.org/10.1002/polb.23025>.
- [23] P. Corsini, et al., Influence of the draw ratio on the tensile and fracture behavior of NMMO regenerated silk fibers, *J. Polym. Sci. Part B Polym. Phys.* 45 (18) (2007) 2568–2579, <https://doi.org/10.1002/polb.21255>.
- [24] H. Venkatesan, J. Chen, J. Hu, Fibers made of recombinant spidroins—a brief review, *AATCC J. Res.* 6, no. 1, suppl (2019) 37–40, <https://doi.org/10.14504/ajr.6.S1.8>.
- [25] Q. Peng, et al., Recombinant spider silk from aqueous solutions via a bio-inspired microfluidic chip, *Sci. Rep.* 6 (1) (2016) 36473, <https://doi.org/10.1038/srep36473>.
- [26] N. Weatherbee-Martin, et al., Identification of wet-spinning and post-spin stretching methods amenable to recombinant spider aciniform silk, *Biomacromolecules* 17 (8) (2016) 2737–2746, <https://doi.org/10.1021/acs.biomac.6b00857>.
- [27] M. Andersson, et al., Biomimetic spinning of artificial spider silk from a chimeric minispidroin, *Nat. Chem. Biol.* 13 (3) (2017) 262–264, <https://doi.org/10.1038/nchembio.2269>.
- [28] S. Ling, Z. Qin, C. Li, W. Huang, D.L. Kaplan, M.J. Buehler, Polymorphic regenerated silk fibers assembled through bioinspired spinning, *Nat. Commun.* 8 (1) (2017) 1387, <https://doi.org/10.1038/s41467-017-00613-5>.
- [29] X. Yue, F. Zhang, H. Wu, J. Ming, Z. Fan, B. Zuo, A novel route to prepare dry-spun silk fibers from CaCl₂-formic acid solution, *Mater. Lett.* 128 (2014) 175–178, <https://doi.org/10.1016/j.matlet.2014.04.116>.
- [30] M. Sun, Y. Zhang, Y. Zhao, H. Shao, X. Hu, The structure–property relationships of artificial silk fabricated by dry-spinning process, *J. Mater. Chem.* 22 (35) (2012) 18372, <https://doi.org/10.1039/c2jm32576d>.
- [31] W. Wei, Y. Zhang, Y. Zhao, J. Luo, H. Shao, X. Hu, Bio-inspired capillary dry spinning of regenerated silk fibroin aqueous solution, *Mater. Sci. Eng. C* 31 (7) (2011) 1602–1608, <https://doi.org/10.1016/j.msec.2011.07.013>.
- [32] J. Luo, et al., Tough silk fibers prepared in air using a biomimetic microfluidic chip, *Int. J. Biol. Macromol.* 66 (2014) 319–324, <https://doi.org/10.1016/j.ijbiomac.2014.02.049>.
- [33] Y. Jin, Y. Zhang, Y. Hang, H. Shao, X. Hu, A simple process for dry spinning of regenerated silk fibroin aqueous solution, *J. Mater. Res.* 28 (20) (2013) 2897–2902, <https://doi.org/10.1557/jmr.2013.276>.
- [34] W. Jin, Y. Zhang, H. Shao, X. Hu, Effects of environment parameters on sol-gel transition and dry-spinnability of regenerated silk fibroin aqueous solution, *Fibers Polym.* 15 (3) (2014) 540–546, <https://doi.org/10.1007/s12221-014-0540-1>.
- [35] S. Weisman, et al., Honeybee silk: recombinant protein production, assembly and fiber spinning, *Biomaterials* 31 (9) (2010) 2695–2700, <https://doi.org/10.1016/j.biomaterials.2009.12.021>.
- [36] B. Schmuck, G. Greco, A. Barth, N.M. Pugno, J. Johansson, A. Rising, High-yield production of a super-soluble miniature spidroin for biomimetic high-performance materials, *Mater. Today* 50 (2021) 16–23, <https://doi.org/10.1016/j.matod.2021.07.020>.
- [37] A. Magaz, et al., Porous, aligned, and biomimetic fibers of regenerated silk fibroin produced by solution blow spinning, *Biomacromolecules* 19 (12) (2018) 4542–4553, <https://doi.org/10.1021/acs.biomac.8b01233>.
- [38] J. Sparkes, C. Holland, Analysis of the pressure requirements for silk spinning reveals a pultrusion dominated process, *Nat. Commun.* 8 (1) (2017) 594, <https://doi.org/10.1038/s41467-017-00409-7>.
- [39] L. Eisoldt, A. Smith, T. Scheibel, Decoding the secrets of spider silk, *Mater. Today* 14 (3) (2011) 80–86, [https://doi.org/10.1016/S1369-7021\(11\)70057-8](https://doi.org/10.1016/S1369-7021(11)70057-8).
- [40] F. Vollrath, D.P. Knight, Structure and function of the silk production pathway in the spider *Nephila edulis*, *Int. J. Biol. Macromol.* 24 (2–3) (1999) 243–249, [https://doi.org/10.1016/S0141-8130\(98\)00095-6](https://doi.org/10.1016/S0141-8130(98)00095-6).
- [41] Teemu Väiläsalmi, Preparation of Regenerated Silk Fibroin Solution and Concentrating With Centrifugal Concentrator Columns, 2023, <https://doi.org/10.5281/ZENODO.8031460>.
- [42] H. Bettahar, T. Väiläsalmi, M. Linder, Q. Zhou, Robotic fiber fabrication based on solidification force control, in: 2022 International Conference on Manipulation, Automation and Robotics at Small Scales (MARSS), IEEE, Toronto, ON, Canada, Jul. 2022, pp. 1–6, <https://doi.org/10.1109/MARSS55884.2022.9870490>.
- [43] H. Bettahar, P.A.D. Harischandra, Q. Zhou, Robotic threading from a gel-like substance based on impedance control with force tracking, *IEEE Robot. Autom. Lett.* 7 (1) (2022) 33–40, <https://doi.org/10.1109/LRA.2021.3116697>.
- [44] A.A.M. André, E. Spruijt, Liquid–liquid phase separation in crowded environments, *Int. J. Mol. Sci.* 21 (16) (2020) 5908, <https://doi.org/10.3390/ijms21165908>.
- [45] P.-H. Peng, K.-W. Hsu, K.-J. Wu, Liquid–liquid phase separation (LLPS) in cellular physiology and tumor biology, *Am. J. Cancer Res.* 11 (8) (2021) 3766–3776.
- [46] S. Alberti, A. Gladfelter, T. Mittag, Considerations and challenges in studying liquid–liquid phase separation and biomolecular condensates, *Cell* 176 (3) (2019) 419–434, <https://doi.org/10.1016/j.cell.2018.12.035>.
- [47] P. Mohammadi, et al., Controllable coacervation of recombinantly produced spider silk protein using kosmotropic salts, *J. Colloid Interface Sci.* 560 (2020) 149–160, <https://doi.org/10.1016/j.jcis.2019.10.058>.
- [48] A.B. Kayitmazer, Thermodynamics of complex coacervation, *Adv. Colloid Interf. Sci.* 239 (2017) 169–177, <https://doi.org/10.1016/j.cis.2016.07.006>.
- [49] L. Lemetti, et al., Liquid–liquid phase separation and assembly of silk-like proteins is dependent on the polymer length, *Biomacromolecules* 23 (8) (2022) 3142–3153, <https://doi.org/10.1021/acs.biomac.2c00179>.
- [50] A. Koeppel, N. Stehling, C. Rodenburg, C. Holland, Spinning Beta silks requires both pH activation and extensional stress, *Adv. Funct. Mater.* 31 (30) (2021), 2103295, <https://doi.org/10.1002/adfm.202103295>.
- [51] R.S. Hoy, Why is understanding glassy polymer mechanics so difficult? *J. Polym. Sci. Part B Polym. Phys.* 49 (14) (2011) 979–984, <https://doi.org/10.1002/polb.22276>.
- [52] M. Joun, I. Choi, J. Eom, M. Lee, Finite element analysis of tensile testing with emphasis on necking, *Comput. Mater. Sci.* 41 (1) (2007) 63–69, <https://doi.org/10.1016/j.commatsci.2007.03.002>.
- [53] L.J. Fetters, D.J. Lohse, D. Richter, T.A. Witten, A. Zirkel, Connection between polymer molecular weight, density, chain dimensions, and melt viscoelastic properties, *Macromolecules* 27 (17) (1994) 4639–4647, <https://doi.org/10.1021/ma00095a001>.
- [54] M. Landreh, et al., Mass spectrometry captures structural intermediates in protein fiber self-assembly, *Chem. Commun.* 53 (23) (2017) 3319–3322, <https://doi.org/10.1039/C7CC00307B>.